Published OnlineFirst August 22, 2012; DOI:10.1158/2159-8290.CD-11-0336

CANCER DISCOVERY

Combining a PI3K Inhibitor with a PARP Inhibitor Provides an Effective Therapy for BRCA1-Related Breast Cancer

Ashish Juvekar, Laura N. Burga, Hai Hu, et al.

Cancer Discovery 2012;2:1048-1063. Published OnlineFirst August 22, 2012.

Published OnlineFirst August 22, 2012; DOI:10.1158/2159-8290.CD-11-0336

RESEARCH ARTICLE

Combining a PI3K Inhibitor with a PARP Inhibitor Provides an Effective Therapy for *BRCA1*-Related Breast Cancer

Ashish Juvekar[1], Laura N. Burga[1], Hai Hu[1], Elaine P. Lunsford[1], Yasir H. Ibrahim[5], Judith Balmañà[5], Anbazhagan Rajendran[1], Antonella Papa[2], Katherine Spencer[1], Costas A. Lyssiotis[3], Caterina Nardella[2], Pier Paolo Pandolfi[2], José Baselga[4,5], Ralph Scully[1], John M. Asara[3], Lewis C. Cantley[3], and Gerburg M. Wulf[1]

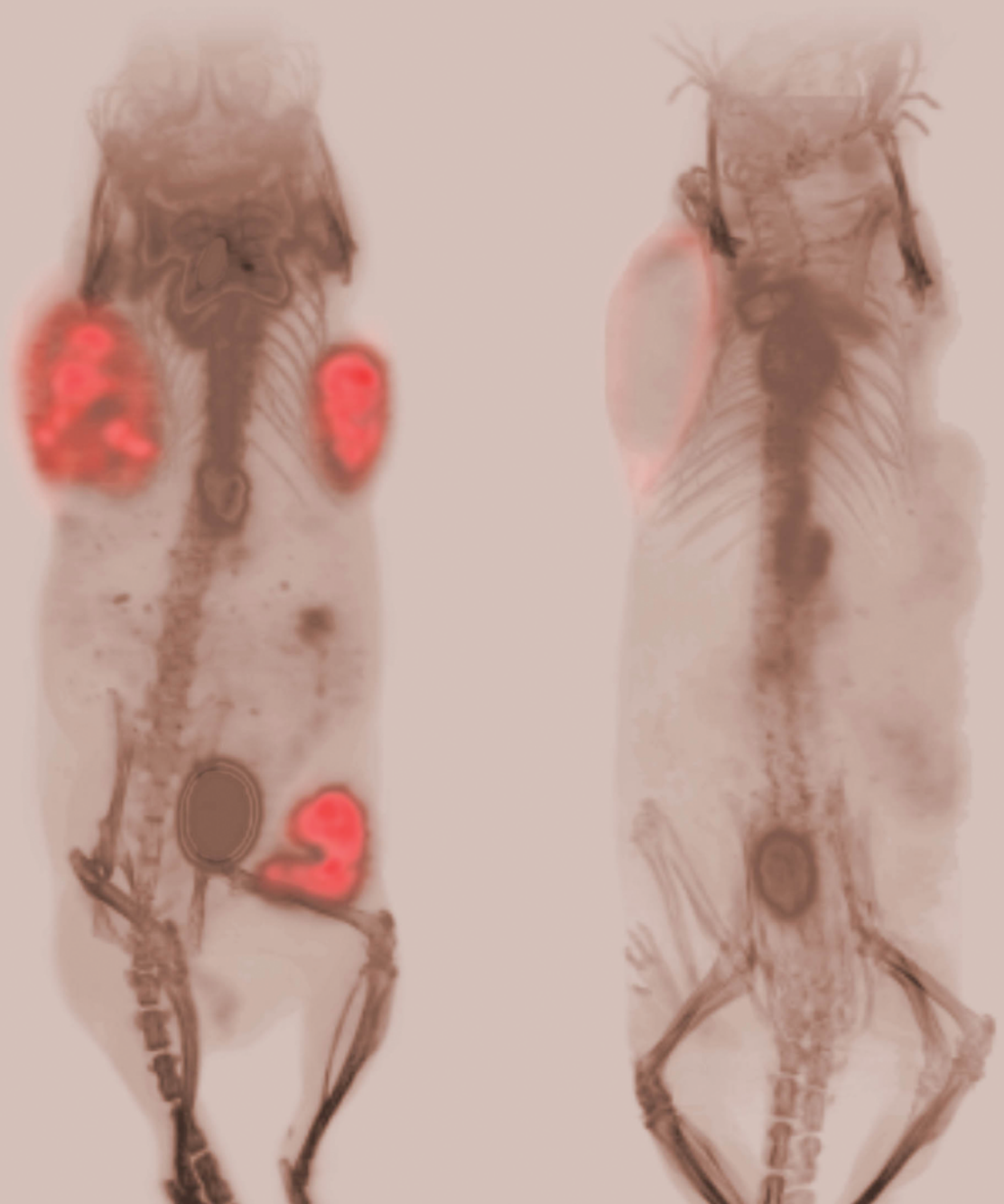

Published OnlineFirst August 22, 2012; DOI:10.1158/2159-8290.CD-11-0336

ABSTRACT There is a need to improve treatments for metastatic breast cancer. Here, we show the activation of the phosphoinositide 3-kinase (PI3K) and mitogen-activated protein kinase (MAPK) pathways in a MMTV-Cre*Brca1*$^{f/f}$*Trp53*$^{+/-}$ mouse model of breast cancer. When treated with the pan-class IA PI3K inhibitor NVP-BKM120, tumor doubling was delayed from 5 to 26 days. NVP-BKM120 reduced AKT phosphorylation, tumor cell proliferation, and angiogenesis. Resistant tumors maintained suppression of AKT phosphorylation but exhibited activation of the MAPK pathway at the "pushing margin." Surprisingly, PI3K inhibition increased indicators of DNA damage, poly-ADP-ribosylation (PAR), and γ-H2AX, but decreased Rad51 focus formation, suggesting a critical role of PI3K activity for Rad51 recruitment. The PARP inhibitor olaparib alone attenuated tumor growth modestly; however, the combination of NVP-BKM120 and olaparib delayed tumor doubling to more than 70 days in the mouse model and more than 50 days in xenotransplants from human *BRCA1*-related tumors, suggesting that combined PI3K and PARP inhibition might be an effective treatment of *BRCA1*-related tumors.

SIGNIFICANCE: Current treatment options for triple-negative breast cancer are limited to chemotherapeutic regimens that have considerable toxicity and are not curative. We report here that the combination of a PI3K inhibitor with a PARP inhibitor provides *in vivo* synergy for treatment of an endogenous mouse model for *BRCA1*-related breast cancers, making this a candidate combination to be tested in human clinical trials. *Cancer Discov; 2(11); 1048–63. ©2012 AACR.*

INTRODUCTION

Unresectable triple-negative breast cancer (TNBC) remains an incurable illness that invariably relapses after treatments considered standard-of-care, leading to death, often within months of diagnosis. Current chemotherapeutic regimens induce not only incomplete remissions that are short but also result in toxicity that severely impacts a patient's quality of life. These shortcomings have led to an extensive search for more effective treatments.

Female *BRCA1* mutation carriers have an approximately 85% lifetime risk of developing breast cancer. These cancers generally are negative for estrogen receptor, progesterone receptor, and HER2 (e.g., triple negative), making them nonresponsive to therapies that target these pathways. Sporadic TNBCs that emerge in patients without germline *BRCA1* or *BRCA2* mutations frequently show evidence for epigenetic silencing of *BRCA1*. Truncating mutations disrupting the C-terminal end of the BRCA1 protein predispose to breast cancer, whereas mutations in the N-terminal two thirds of the protein result in elevated susceptibility to both breast and ovarian cancer (1).

Loss of *BRCA1* in breast epithelial cells disables DNA damage repair via homologous recombination. This defect leads to genomic instability but also sensitizes cells to the deleterious effects of other DNA-damaging agents, such as cisplatin or inhibitors of poly-ADP-ribosylation (PAR). Poly (ADP-ribose) polymerase (PARP) is a nuclear enzyme that senses DNA single-strand breaks and is essential for base excision repair. Once base excision repair is disabled, cells rely on homologous recombination for DNA damage repair. Dysfunction of homologous recombination (such as in *BRCA1*-deficient cells) presents a context in which inhibition of base excision repair (e.g., by treating with PARP inhibitors) is synthetically lethal. Clinically, PARP inhibitors have emerged as promising agents, inducing objective responses in 41% of patients with *BRCA1*-related breast cancer (2, 3) and 33% of patients with *BRCA1*-related ovarian cancer (4, 5). However, the remissions achieved with PARP inhibitors have not been durable, and benefit in the subset of TNBCs that are not *BRCA1*-related is currently uncertain.

Multiple lines of evidence suggest that growth factor signaling may be a sensible target for the treatment of TNBC: EGF receptor (EGFR) overexpression seems to correlate with the basaloid phenotype and is found in 60% to 70% of TNBCs, including *BRCA1*-related cancers (6). We have previously shown that upregulation of EGFR and the EGF pathway is an early event in *BRCA1*-related tumorigenesis (7). IGF-1R levels are increased in *BRCA1*-related breast cancers (8) and genetic variants in the insulin-like growth factor (IGF) pathway are associated with *BRCA1*-related tumorigenesis (9, 10). However, VEGF receptor (VEGFR) and EGFR inhibitors, alone or in combination with traditional chemotherapy, have

Authors' Affiliations: Divisions of [1]Hematology and Oncology, [2]Cancer Genetics, and [3]Signal Transduction, Beth Israel Deaconess Medical Center and Department of Medicine, Harvard Medical School; [4]Division of Hematology/Oncology, Massachusetts General Hospital, Boston, Massachusetts; and [5]Medical Oncology Department, University Hospital Vall d'Hebron, Paseo Vall d'Hebron, Barcelona, Spain

Note: Supplementary data for this article are available at Cancer Discovery Online (http://cancerdiscovery.aacrjournals.org/).

L.N. Burga and H. Hu contributed equally to this work.

Corresponding Author: Gerburg M. Wulf, Division of Hematology and Oncology, Beth Israel Deaconess Medical Center, 330 Brookline Avenue, Boston, MA 02215. Phone: 617-667-1910; Fax: 617-667-1960; E-mail: gwulf@bidmc.harvard.edu

doi: 10.1158/2159-8290.CD-11-0336

Published OnlineFirst August 22, 2012; DOI:10.1158/2159-8290.CD-11-0336

not improved survival for patients with TNBC. One explanation for this lack of efficacy is that resistant tumor cells signal through alternate receptor tyrosine kinases, turning the search for new therapeutic angles to nodal points of intracellular signal transduction, such as mitogen-activated protein kinase (MAPK) and phosphoinositide 3-kinase (PI3K), in which inhibition may be harder for tumor cells to evade. Here, we examine the mechanism and the efficacy of a PI3K inhibitor, NVP-BKM120, for the treatment of *BRCA1*-related breast cancer in a mouse model and report on a surprising *in vivo* synergy with PARP inhibition.

RESULTS

Activation of the PI3K Pathway in *BRCA1*-Related Breast Cancer

We and others have previously shown that the MMTV-Cre*Brca1*$^{f/f}$*Trp53*$^{+/-}$ mouse model faithfully recapitulates many aspects of human *BRCA1*-related breast cancer, including emergence on a background of multiple synchronous hyperproliferative lesions, high proliferative activity, absence of estrogen receptor expression, and the presence of EGFR overexpression (11–14), although exon 11 deletion in this model results in the residual expression of a hypomorphic BRCA1 protein, rather than complete absence of the *BRCA1* protein shown in other models (15).

BRCA1 has been shown to suppress AKT (16) and extracellular signal-regulated kinase (ERK) activation in response to estrogen or EGF stimulation (17, 18) in cell-based studies, suggesting that tumors with defects in *BRCA1* might have an increase in AKT and/or ERK phosphorylation. Consistently, we found that phosphorylation of AKT at Serine 473 was strongly positive in both the cytoplasm and the nucleus in these tumor cells (Fig. 1, top right, and Supplementary Fig. S1), whereas in the normal adjacent tissue, cytoplasmic AKT phosphorylation was only seen in the basal layer of cells, not in luminal cells (Fig. 1, top left). Similarly, ERK phosphorylation was absent in normal mammary epithelial cells, whereas cytoplasmic ERK phosphorylation was seen in a majority of but not in all tumor cells (Fig. 1, second panel).

Loss of function of *PTEN*, either through epigenetic silencing or through gross genomic loss, correlates with loss of function of *BRCA1* in TNBC (19). Recently, Gewinner and colleagues (20) as well as Fedele and colleagues (21) showed that, similar to *PTEN*, the tumor suppressor phosphatase *INPP4B* is lost in approximately 60% of TNBC, including *BRCA1*-related breast cancers. Consistent with these data in human disease, INPP4B and PTEN expression were strong in normal glands of MMTV-Cre*Brca1*$^{f/f}$*Trp53*$^{+/-}$ females but lost in tumor tissues (Fig. 1, third panel and bottom).

To examine whether activating *PIK3CA* mutations are responsible for the strong and uniform activation of AKT, we sequenced the *Pik3ca* gene of 11 murine *Brca1*-deleted breast tumors. Consistent with the rarity of mutations in human TNBC, we found no activating hotspot mutations in exons 9 or 20 of PI3K. In human TNBC, activating mutations in *Pik3ca* are relatively rare and seen in only 8% of TNBC, confirming that the activation of the PI3K pathway in TNBC is mostly driven by regulatory mechanisms, such as loss of *PTEN* and *INPP4B*, rather than by activating mutations in *PIK3CA*.

Collectively, these observations suggest that the MMTV-Cre*Brca1*$^{f/f}$*Trp53*$^{+/-}$ mouse model accurately recapitulates the activation of growth factor signaling seen in human *BRCA1*-related breast cancer, including activation of the PI3K and MAPK pathways and the absence of activating PI3K mutations. On the basis of these data, we decided to study whether inhibition of PI3K would be an effective treatment of *BRCA1*-related breast cancer.

Pharmacodynamics of PI3K Inhibition in *BRCA1*-Related Breast Cancer

TNBCs, including the *BRCA1*-related subtype, exhibit high rates of glucose uptake, as judged by positron emission tomography (PET) using the radioactive glucose analog, 2[^{18}F] fluoro-2-deoxy-D-glucose (FDG; refs. 22, 23). Consistent with these observations in humans, we found that *Brca1*-deleted tumors in our mouse model were highly avid for FDG. Tumors of subcentimeter size were easily visualized using this technique (Fig. 2; Supplementary Figs. S2 and S3). In a previous study (24), mouse lung tumors that resulted from transgenic expression of the H1047R mutant of PIK3CA were found to have high rates of glucose uptake as judged by FDG-PET, and the PI3K/mTOR inhibitor BEZ235 caused a reduction in the FDG-PET signal within 2 days, consistent with the known role of PI3K in regulating glucose uptake and glycolysis (25–27). We found that within 48 hours of instituting treatment with NVP-BKM120, tumors in all treated animals showed a median decrease in FDG uptake by 46.7% (range, 38.1–92.3), which was sustained after 2 weeks of continued treatment with NVP-BKM120 (median decrease by 54%, range 45.5%–70.5%) and corresponded to inhibition of AKT phosphorylation (Fig. 2A–D, Supplementary Figs. S2 and S3). These results indicate that the activation of the PI3K pathway contributes to the upregulation of glucose metabolism in *BRCA1*-related breast cancers and that oral delivery of NVP-BKM120 results in inhibition of this response. Further evidence that NVP-BKM120 inhibits PI3K signaling in the *Brca1*-defective tumors was provided by the observation that phosphorylation of the downstream protein kinase AKT at Ser-473 was strongly decreased in tumors treated with NVP-BKM120 (Fig. 2B, Supplementary Fig. S1). It was remarkable that all *Brca1*-related tumors examined showed a decrease in FDG uptake and a decrease in AKT phosphorylation in response to NVP-BKM120 (Fig. 2, Supplementary Figs. S2 and S3), suggesting that a high level of PI3K signaling and the consequent enhanced glucose metabolism is a common event in tumors that result from loss of BRCA 1 function. In addition, our data suggest that inhibition of FDG uptake may be an early and predictive pharmacodynamic marker for response to treatments with PI3K inhibitors.

The PI3K Inhibitor NVP-BKM120 Exerts Antiangiogenic Activity

Tumor growth requires neovascularization of the expanding neoplastic tissue. It was previously shown that BEZ235, a PI3K inhibitor with activity against PI3Kα and mTOR, inhibits the sprouting of new blood vessels in tumors and disrupts the integrity of existing blood vessels (27, 28). Spontaneous tumors in MMTV-Cre*Brca1*$^{f/f}$*Trp53*$^{+/-}$ mice

Published OnlineFirst August 22, 2012; DOI:10.1158/2159-8290.CD-11-0336

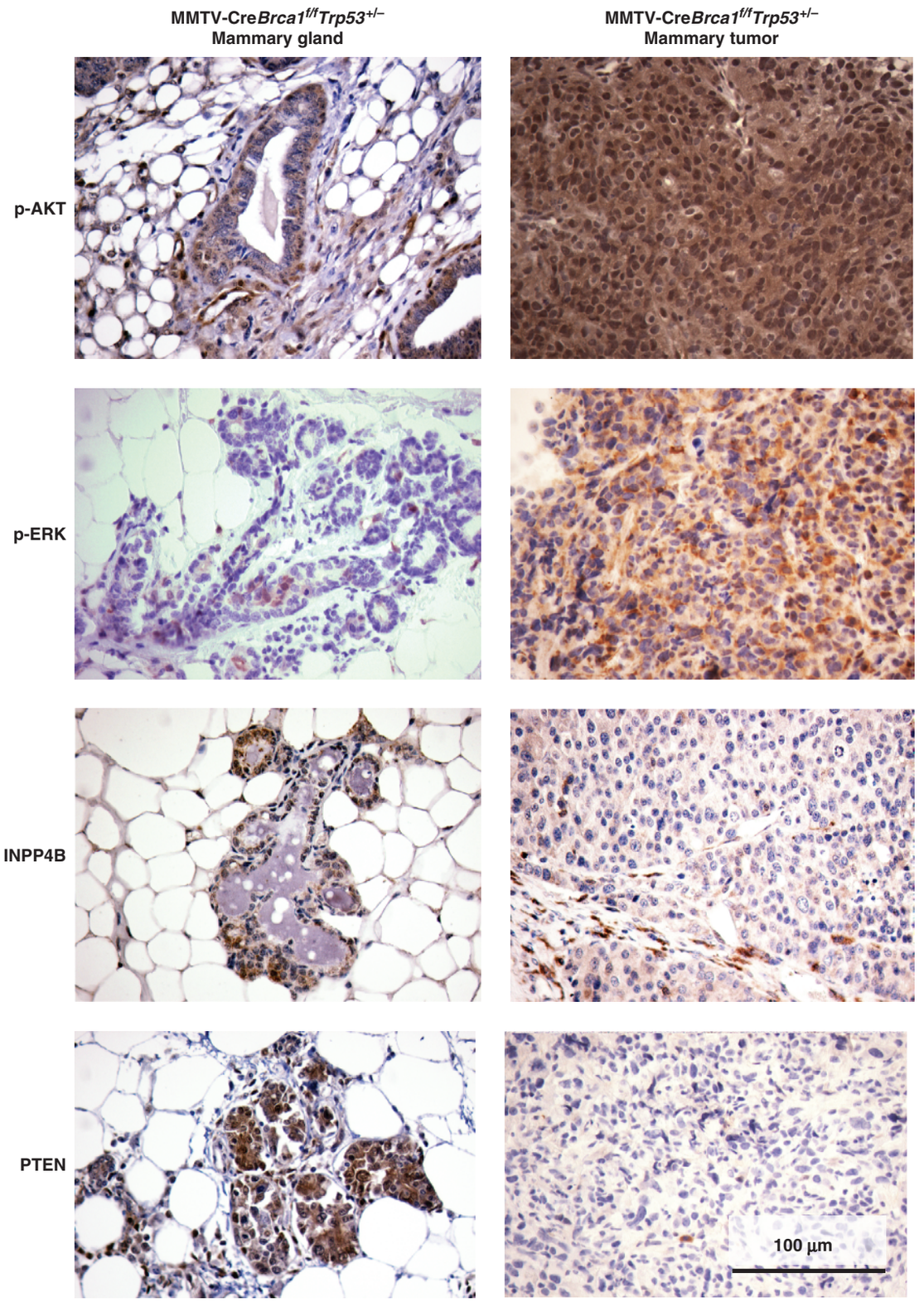

Figure 1. PI3K pathway activation in *BRCA1*-related breast cancer in MMTV-Cre*Brca1*$^{f/f}$*Trp53*$^{+/-}$ mice. Tumor-bearing females were euthanized, and tissues were harvested and processed for immunohistochemistry (IHC). Displayed are representative images of IHC for phospho-AKT (S473), phosphorylated ERK (Thr202/Tyr204) and the tumor-suppressor phosphatases INPP4B and PTEN. Adjacent normal mammary gland tissue is on the left, tumor tissue on the right. ×400 magnification.

Published OnlineFirst August 22, 2012; DOI:10.1158/2159-8290.CD-11-0336

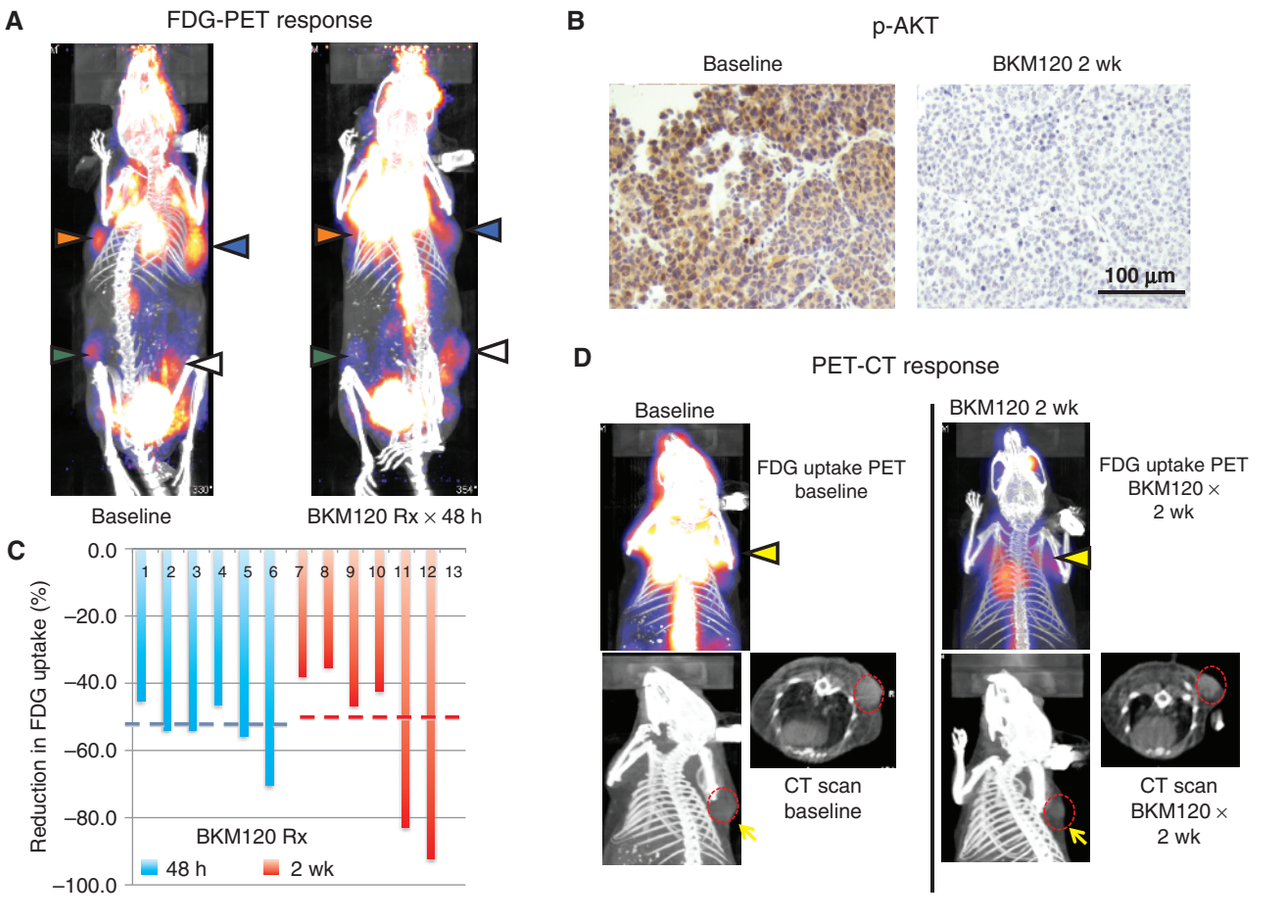

Figure 2. Pharmacodynamic effects of PI3K inhibitor NVP-BKM120 on breast carcinomas in MMTV-Cre*Brca1*$^{f/f}$*Trp53*$^{+/-}$ mice. Female virgin mice developed spontaneous breast cancers at ages 8 to 12 months. **A,** representative ^{18}FDG PET–CT scan images of a tumor-bearing mouse at baseline (image on the left) and within 48 hours after starting treatments with the PI3K inhibitor NVP-BKM120 (50 mg/kg/d by gavage, image on the right). This mouse had developed 4 simultaneous tumors. Arrows in orange, green, blue, and white are used to identify different tumors upon baseline (left) and post-treatment (right) imaging. The color palette for uptake ranges from dark blue to bright yellow with increasing count intensity. The changes in FDG uptake were determined as described in Methods. They decreased by 45% (tumor with orange arrow), 64% (green arrow), 64% (blue arrow), and 56% (white arrow). **B,** suppression of AKT phosphorylation on S473 as a result of treatments with NVP-BKM120 *in vivo*. Tumor tissue was obtained via core needle biopsy before and after 2 weeks of treatments with NVP-BKM120, fixed, and processed for IHC with anti-pAKT (S473) antibodies. For additional IHC images, see Supplementary Fig. S1. **C,** decrease in FDG uptake in 6 mammary carcinomas. Relative decrease in FDG uptake was determined by the ratio of uptake at 48 hours (blue bars) or 2 weeks (red bars) to baseline. Tumor-specific FDG uptake was determined as described in Methods. For additional PET–CT images, see Supplementary Fig. S2. **D,** concordance of decrease in FDG uptake and tumor shrinkage during a 2-week treatment with PI3K inhibitor NVP-BKM120. The tumor-bearing animal was imaged with FDG-PET (top, tumor indicated with a yellow arrow before and after treatment, decrease in uptake 93%) and concomitant CT scan (bottom) before (left) and on treatment (right). The tumor is again marked in the CT scan with a yellow arrow in the axial and sagittal plane. The red outline indicates the tumor circumference before treatment to visualize treatment effect on tumor size.

grow rapidly and are highly vascular (Fig. 3A, left; Fig. 3B). However, after treatment with NVP-BKM120, the gross pathology of tumors was notable for central pallor and, eventually, central necrosis (Fig. 3A, middle). In contrast, blood vessels in the tumor capsule remained initially intact, or became ectatic (Fig. 3A). Consistently, the tumor microvasculature, as visualized with an anti-CD31 stain, was diminished in response to NVP-BKM120 (Fig. 3C) while it was maintained in the tumor capsule (Fig. 3D). The necrotic center of treated tumors was frequently hemorrhagic (data not shown), indicating disorganized collapse of the tumor vasculature. We used the Chalkley count of CD31-positive microvessels (29) to compare the vascularization before and after treatment with NVP-BKM120 and found that both the size and number of blood vessels were starkly reduced in treated tumors (Fig. 3E). Thus, consistent with prior observations with BEZ235 (28) and recent data with NVP-BKM120 (30), our data confirm that NVP-BKM120's antitumor activity is, in part, due to its antiangiogenic activity, and thus this drug may have preferential activity in rapidly growing, endocrine-resistant tumors with a high degree of tumor angiogenesis.

Effects of PI3K Inhibition on Compensatory Pathways in Tumor Cells

The upregulation of compensatory pathways in response to tumor cell treatments with inhibitors of mitogenic signaling is now a well-known phenomenon (31). Consistent with these

Published OnlineFirst August 22, 2012; DOI:10.1158/2159-8290.CD-11-0336

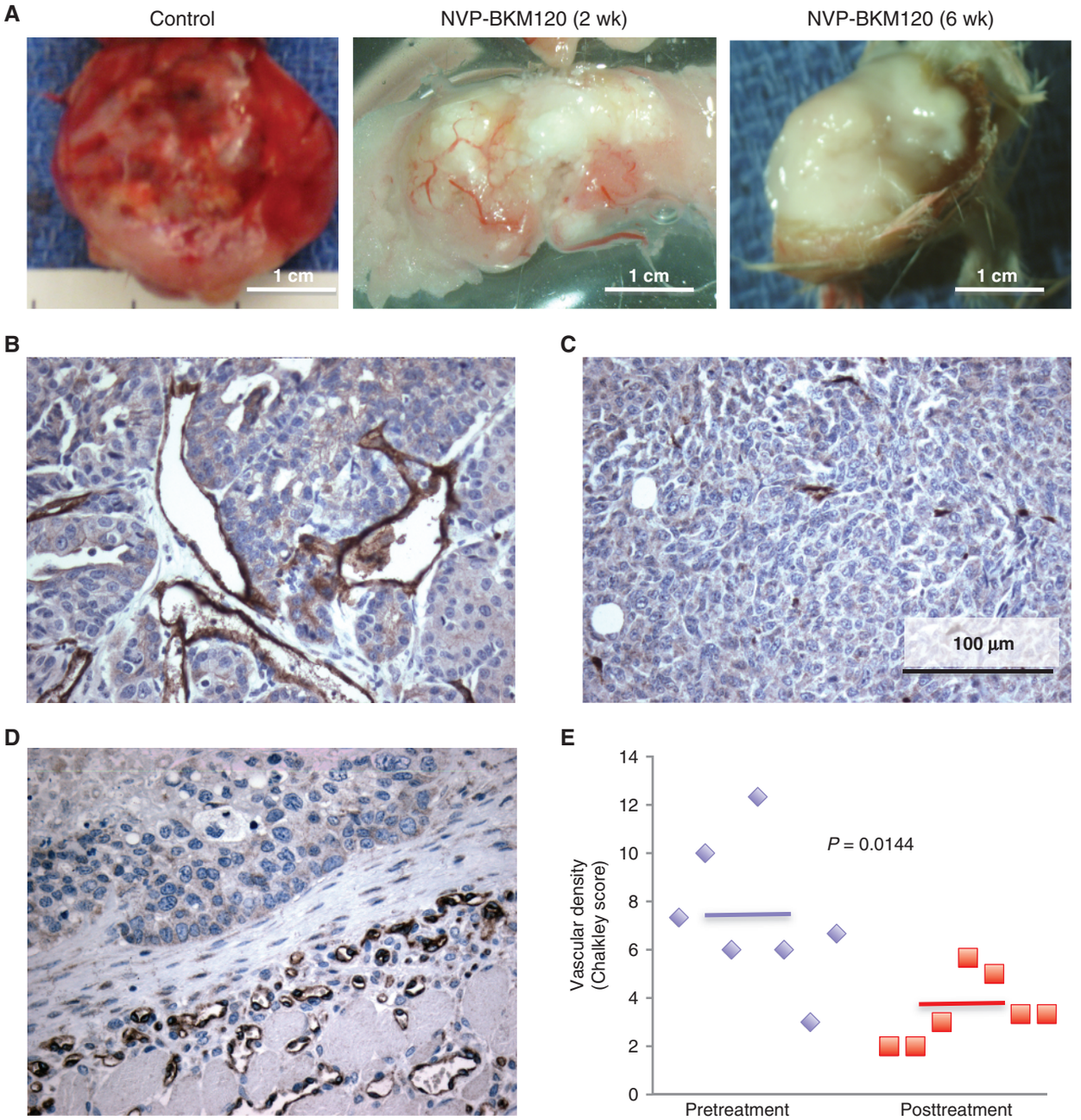

Figure 3. Antiangiogenic effects of PI3K inhibitor NVP-BKM120. **A,** gross pathologic images of an untreated tumor (left), a tumor treated for 2 weeks (middle), and a tumor treated for 6 weeks (right) with NVP-BKM120 at 50 mg/kg/d via gavage. IHC to detect CD31 in an untreated tumor (**B**), the center of a tumor treated for 6 weeks (**C**), and the tumor capsule of a mammary tumor treated for 6 weeks (**D**). **E,** determination of the Chalkley score to quantify CD31 staining. IHC with anti-CD31 antibodies was conducted in pretreatment biopsies and in tumor specimens from mice at the time of tumor progression.

prior observations, we found that NVP-BKM120 induced a compensatory activation of the EGFR/MAPK pathways in the human *BRCA1*-mutant breast cancer cell lines, HCC1937 (BRCA1 5382C mutation and homozygous deletion of *PTEN* and *TP53*; ref. 32), and SUM149 (*BRCA1* 2288delT, *PTEN* wild type, *TP53* mutant; refs. 33, 34; Fig. 4A, second lane for each cell line). As expected, treatments with the PARP inhibitor olaparib alone did not have a discernible effect on the activation status of EGFR, AKT, or MAPK (Fig. 4A, third lane for each cell line). However, with the combination treatment (Fig. 4A, last lane), we found that compensatory activation of EGFR and MAPK could be blocked by the addition of olaparib. These data suggest that PARP inhibition in tumor cells either restricts mitogenic signaling to PI3K-mediated signaling, or disables mechanisms that would reroute mitogenic signaling via EGFR/ERK when PI3K is inhibited.

Published OnlineFirst August 22, 2012; DOI:10.1158/2159-8290.CD-11-0336

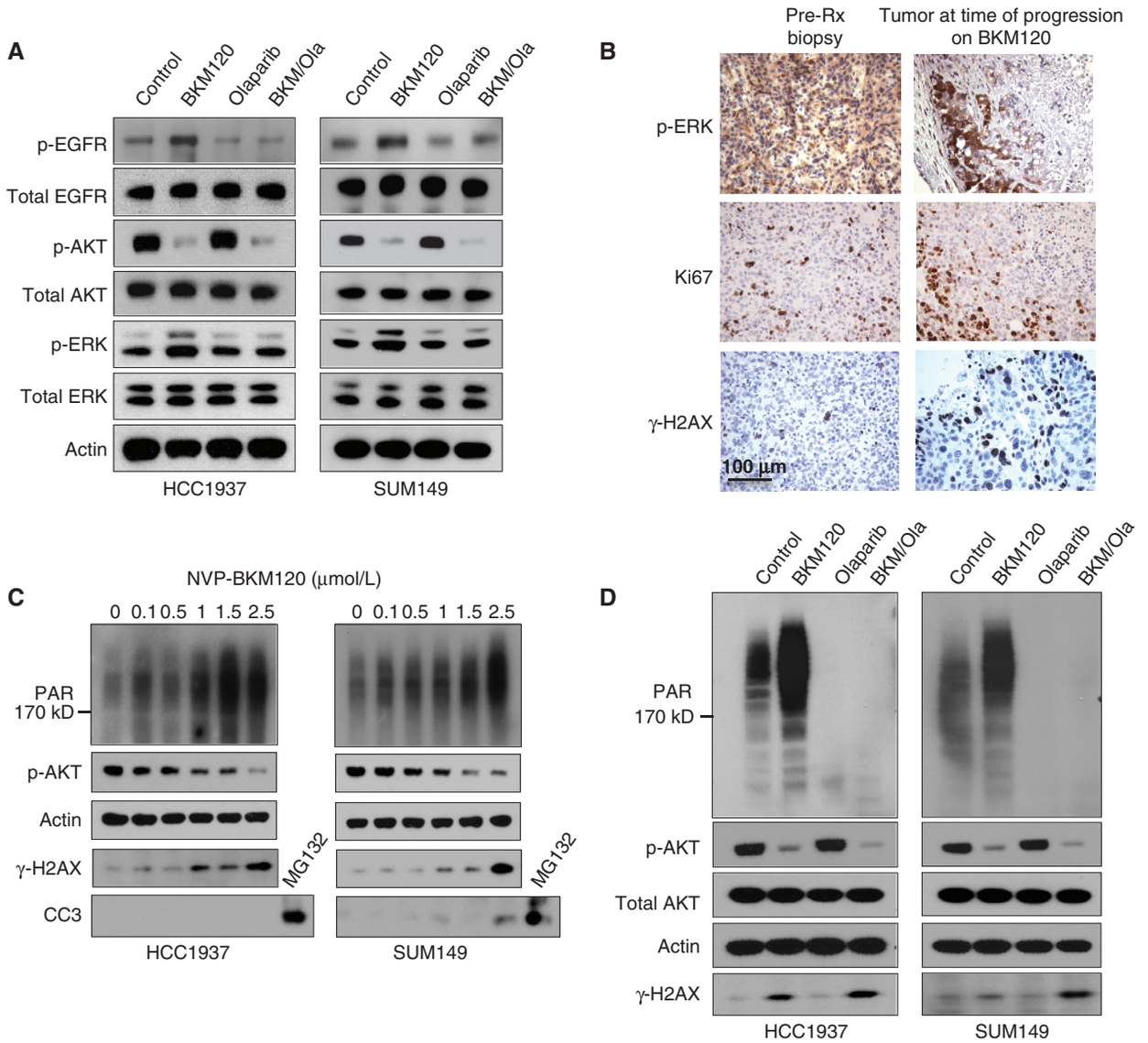

Figure 4. PI3K inhibition increases PAR and H2AX phosphorylation. **A,** compensatory pathway activation induced by treatments with NVP-BKM120. HCC1937 or SUM149 cells were treated with NVP-BKM120, olaparib, or its combination as indicated for 72 hours, lysed, and subjected to immunoblotting with antibodies against total AKT, EGFR, ERK and their phospho-specific epitopes. **B,** *in vivo* increase of γ-H2AX–positive cells after treatment with NVP-BKM120 and proliferative activity at the "pushing margin." Tumor-bearing mice were subjected to a pretreatment biopsy and then treated with NVP-BKM120 at 50 mg/kg/d. IHC of pretreatment biopsies and posttreatment tumor tissues was conducted with antibodies as indicated. **C,** *BRCA1*-mutant human HCC1937 or SUM149 cells were treated with vehicle control or NVP-BKM120 at the indicated concentrations for 24 hours, lysed, and subjected to immunoblotting with antibodies against PAR, phosphorylated AKT (p-AKT; S473), γ-H2AX, CC3 as an apoptosis marker, and actin as a loading control. **D,** effects of combined PI3K and PARP inhibition on *Brca1*-mutant cells. Cells were treated with NVP-BKM120 at 1 μmol/L and olaparib at 10 μmol/L or their combination for 24 hours, lysed, and subjected to immunoblotting with antibodies against PAR, p-AKT, total AKT, γ-H2AX, and actin as indicated. p-EGFR, phosphorylated ERK.

Treatments with NVP-BKM120 Increase Indicators of DNA Damage but Decrease Rad51 Recruitment to Repair Foci

Loss of BRCA1 function results in genome instability due to defects in DNA repair by homologous recombination. As a consequence, *BRCA1*$^{-/-}$ cells have high rates of DNA damage and are sensitized to the inhibition of alternative DNA repair mechanisms involving PARP-dependent PAR (34). We examined the possibility that the high sensitivity of *BRCA1*-mutant tumors to PI3K pathway inhibitors is the consequence of a role for the PI3K pathway in maintaining cell survival during DNA repair or in facilitating DNA repair mechanisms. These experiments were carried out *in vivo* (Fig. 4B) and with the human *BRCA1*-mutant cell lines, HCC1937 and SUM149. We first examined the effect of NVP-BKM120 on DNA repair responses in cells grown on plastic. Surprisingly, we found that in both cell lines, histone 2AX (H2AX) phosphorylation

Published OnlineFirst August 22, 2012; DOI:10.1158/2159-8290.CD-11-0336

on Serine 139 (γ-H2AX, a marker for DNA double-strand damage) increased with increasing concentrations of NVP-BKM120 and that this correlated with diminishing phosphorylation of AKT (Fig. 4C). Similarly, tumors treated with NVP-BKM120 *in vivo* showed a substantial increase in the percentage of cells that express γ-H2AX (Fig. 4B).

Tumors with loss of *BRCA1* rely on PARP-dependent PAR of key proteins involved in DNA damage repair (34). Given the surprising increase in H2AX phosphorylation, we examined if treatment with NVP-BKM120 would also affect PARP activity. Treatment with NVP-BKM120 caused a dose-dependent increase in overall PAR that paralleled the increase in H2AX phosphorylation and the decrease in AKT phosphorylation (Fig. 4C). Importantly, this increase in PAR was initially not accompanied by apoptotic cell death, as cells remained negative for cleaved caspase-3 (CC3; Fig. 4C). The basal and NVP-BKM120–enhanced PAR could be completely blocked by treatment with the PARP inhibitor, olaparib (Fig. 4D), whereas γ-H2AX accumulation was enhanced with the combination of NVP-BKM120 and olaparib (Fig. 4D).

Thus, we observed that PI3K inhibition caused a significant increase in activities indicative of both types of DNA damage: PARP activity, which is required for base excision repair and single-strand break repair, as well as H2AX phosphorylation, indicative of the presence of DNA double-strand breaks (DSB). As H2AX is a substrate for the PI3K-related kinases Ataxia teleangiectasia mutated (ATM) and DNA-dependent protein kinase (DNA-PK), we asked if NVP-BKM120 had an effect on these kinases that would explain our findings. We examined PAR and γ-H2AX accumulation in HCC1937 cells in the absence and presence of the ATM-inhibitor KU-55933 (35) and monitored the response to ionizing radiation. As expected, KU-55933 led to a decrease in autophosphorylation of ATM (Fig. 5A, third and fourth lane of each panel), and prevented the increase in H2AX phosphorylation seen in response to ionizing radiation. However, KU-55933 did not prevent the NVP-BKM120–induced induction of γ-H2AX, which was robust both at baseline and in response to ionizing radiation (Fig. 5A, last lane of each panel), suggesting that an alternative kinase, such as DNA-PK, phosphorylates H2AX in response to PI3K inhibition. As shown in Fig. 5A, we found a strong increase in autophosphorylation of DNA-PK in response to the addition of NVP-BKM120 that corresponds to H2AX phosphorylation. Consistent with prior reports (30), these results clearly show that NVP-BKM120 is not acting through an off-target inhibition of ATM or DNA-PK and suggest that inhibition of PI3K by NVP-BKM120 leads to the activation of DNA-PK through a yet unknown mechanism.

Consistent with the results in Fig. 4C, we found that PAR accumulation in the presence of NVP-BKM120 alone increased (Fig. 5A, left, second lane). In the presence of the combination of NVP-BKM120 and KU-55933, PAR accumulation was attenuated but still greater than in the control, suggesting that the NVP-BKM120–induced increase in PAR was only partially offset by inhibition of ATM, again consistent with an ATM-independent mechanism for PAR-accumulation and its induction by PI3K inhibition.

To determine if PI3K inhibition affected the assembly of DNA damage repair foci, we examined the ability of tumor cells from our mouse model to recruit Rad51 to DNA damage repair foci (Fig. 5B–E), following a protocol established previously (36). We generated cell cultures from tumors of MMTV-Cre*Brca1*$^{f/f}$*Trp53*$^{+/-}$ mice and examined their ability to form DNA repair foci 6 hours after exposure to ionizing radiation (10 Gy). We found that there was residual double-strand repair activity as shown by the formation of Rad51 foci in this mouse model with a hypomorphic exon 11 deletion (Fig. 5C). Surprisingly, the formation of Rad51 foci in response to ionizing radiation was completely blocked by pretreatment of these cells with NVP-BKM120 (Fig. 5E). A similar phenomenon was observed in HCC1937 cells: although ionizing radiation induced accumulation of Rad51 and H2AX phosphorylation as reported previously (ref. 37; Fig. 5A, control lanes), pretreatment with the PI3K inhibitor NVP-BKM120 led to a dissociation of this radiation response, as we saw a failure to increase Rad51 but a prominent augmentation of radiation-induced H2AX phosphorylation in the presence of NVP-BKM120 (Fig. 5A, second lane of each panel). The mechanism by which NVP-BKM120 decreases Rad51 recruitment to repair foci is yet unknown. However, this observation of a defective DSB repair response may, at least in part, provide an additional explanation for the *in vivo* synergy of PARP and PI3K inhibition.

Effects of NVP-BKM120 Are Specific for PI3Kα Inhibition

Given the unanticipated and striking effects of the pan-class IA PI3K inhibitor NVP-BKM120 on the DNA damage response, we asked whether these effects were specific to a single class IA PI3K isoform or required inhibition of multiple PI3Ks or could be an off-target effect of NVP-BKM120. In the *BRCA1*-mutant cell line SUM149, downregulation of PI3Kα, but not PI3Kβ, with siRNA led to a stark increase in phosphorylation of DNA-PK, γ-H2AX, and PAR, and a stark decrease in Rad51 accumulation (Fig. 5F). These data confirm that it is the inhibition of PI3Kα that is decisive for the disruption of the DNA damage response in these cells.

Therapeutic Efficacy of the PI3K Inhibitor NVP-BKM120 Alone and in Combination with the PARP Inhibitor Olaparib

We first examined the effect of NVP-BKM120 and olaparib on the growth on plastic of the 2 *BRCA1*-mutant cell lines. HCC1937 cells, with a genetic loss of *PTEN*, showed greater sensitivity to NVP-BKM120 than SUM149 cells, which have wild-type *PTEN* (Supplementary Fig. S4A). SUM149, on the other hand, showed greater sensitivity to olaparib (Supplementary Fig. S4B). The drug combination did not have much benefit beyond that of the most effective single agent in either cell line (Supplementary Fig. S4) and isogenic reconstitution of PTEN in HCC1937 did not significantly alter drug sensitivities (Supplementary Fig. S4C and S4D), indicating that under the artificial conditions of growth on plastic with high levels of nutrients and oxygen, and in the absence of the native tumor microenvironment, this drug combination does not result in synergy. We next addressed whether NVP-BKM120 and olaparib might have a more dramatic effect *in vivo* on endogenous *BRCA1*-deleted tumors. We first showed that, consistent with the observations with the human *BRCA1*-mutant cell lines, NVP-BKM120 treatment of mice with *Brca1*-deleted breast tumors (MMTV-Cre*Brca1*$^{f/f}$*Trp53*$^{+/-}$) resulted in an increase in phosphorylated H2AX in the recurrent tumors (Fig. 4B).

Published OnlineFirst August 22, 2012; DOI:10.1158/2159-8290.CD-11-0336

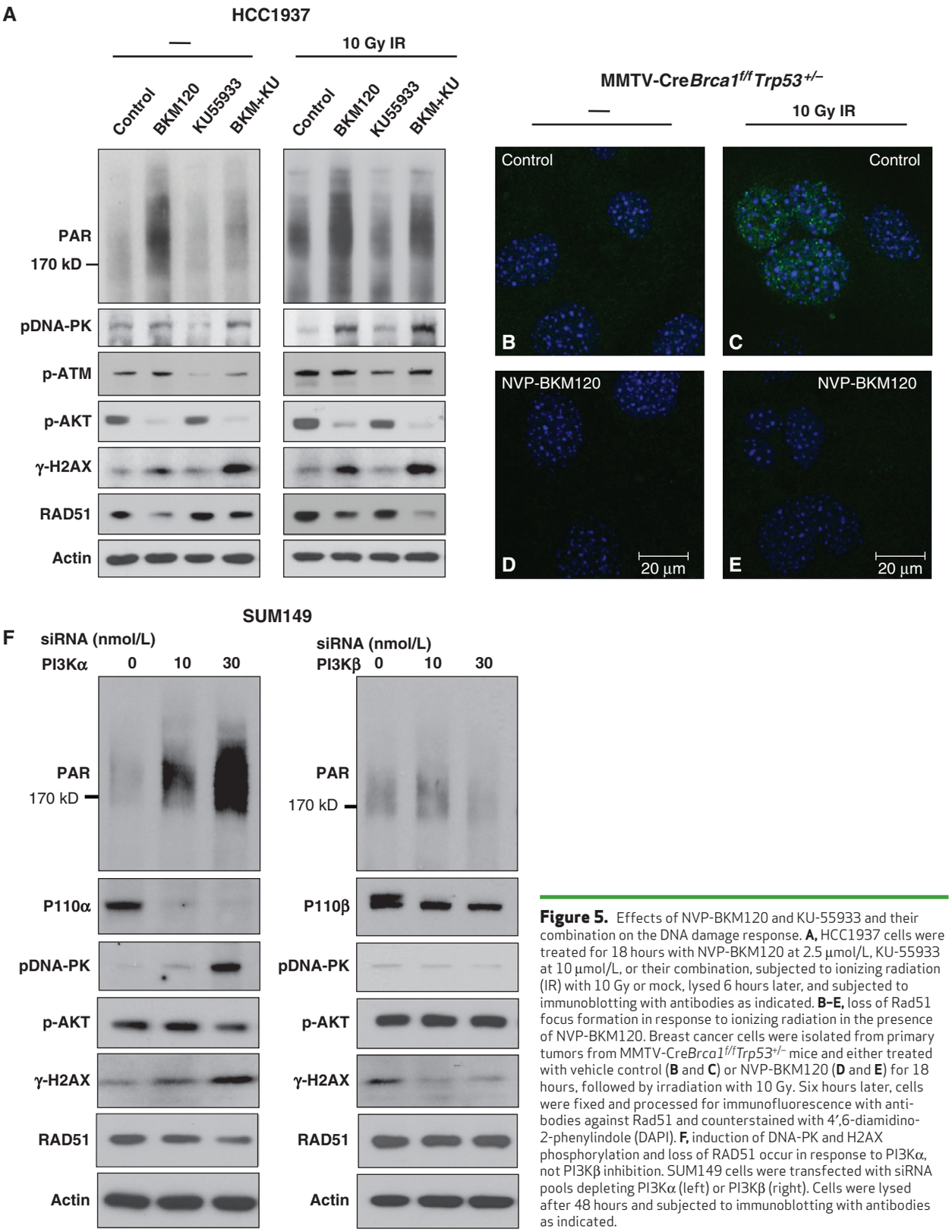

Figure 5. Effects of NVP-BKM120 and KU-55933 and their combination on the DNA damage response. **A,** HCC1937 cells were treated for 18 hours with NVP-BKM120 at 2.5 μmol/L, KU-55933 at 10 μmol/L, or their combination, subjected to ionizing radiation (IR) with 10 Gy or mock, lysed 6 hours later, and subjected to immunoblotting with antibodies as indicated. **B–E,** loss of Rad51 focus formation in response to ionizing radiation in the presence of NVP-BKM120. Breast cancer cells were isolated from primary tumors from MMTV-Cre*Brca1*$^{f/f}$*Trp53*$^{+/-}$ mice and either treated with vehicle control (**B** and **C**) or NVP-BKM120 (**D** and **E**) for 18 hours, followed by irradiation with 10 Gy. Six hours later, cells were fixed and processed for immunofluorescence with antibodies against Rad51 and counterstained with 4′,6-diamidino-2-phenylindole (DAPI). **F,** induction of DNA-PK and H2AX phosphorylation and loss of RAD51 occur in response to PI3Kα, not PI3Kβ inhibition. SUM149 cells were transfected with siRNA pools depleting PI3Kα (left) or PI3Kβ (right). Cells were lysed after 48 hours and subjected to immunoblotting with antibodies as indicated.

We next compared the effects of NVP-BKM120 and olaparib as single agents and the combination of both drugs on tumor growth. Female virgin MMTV-Cre*Brca1*$^{f/f}$*Trp53*$^{+/-}$ mice were observed for the development of spontaneous tumors, which typically occurs at age 8 to 12 months. Once tumors reached a diameter of 5 to 7 mm, mice were randomized to either vehicle control treatments, treatments with NVP-BKM120 via oral gavage, olaparib intraperitoneally, or the combination of NVP-BKM120 with olaparib, all once a day continuously. An initial set of mice was treated with NVP-BKM120 at 50 mg/kg/d, alone or in combination with olaparib (50 mg/kg/d) and a second set at NVP-BKM120 30 mg/kg/d alone or in combination with olaparib (50 mg/kg/d). No significant difference was seen with regard to efficacy or phosphorylated AKT (p-AKT) suppression between the 2 dose levels of NVP-BKM120 and data were pooled (Fig. 6A–D). Tumors were measured at least 3 times a week, and relative tumor volume, as a ratio to baseline tumor volume, was calculated for each treatment modality (Fig. 6A–D). Trend lines were determined on the basis of the best fit to the data in vehicle control (red line) and NVP-BKM120 only (green line). Once tumors were established, their doubling time was rapid if treated with vehicle only, on average 5 days (Fig. 6A). Treatment with NVP-BKM120 alone significantly prolonged tumor-doubling time by a factor of 5 (26 days vs. 5 days, Fig. 6B); however, tumors eventually grew (Fig. 6B). In this mouse model, tumor growth was delayed 3-fold with the use of olaparib (tumor doubling time 16 days vs. 5 days; Fig. 6C). When olaparib and NVP-BKM120 were combined, we found a surprising *in vivo* synergistic activity, with a tumor doubling time of over 70 days, a 14-fold increase over control (red trend line). The dual combination of NVP-BKM120 and olaparib did not result in measurable toxicity, such as weight loss (Fig. 6E), even in mice that were treated for over 3 months. To ensure target inhibition, we obtained pretreatment biopsies and matched tumor specimens within 2 hours of the last dose of NVP-BKM120 and found that NVP-BKM120 potently reduced AKT phosphorylation (Fig. 6F and Supplementary Fig. S1). In tumor tissue lysates from the combination treatment, we observed inhibition of p-AKT with the combination treatment and induction of γ-H2AX (Fig. 6F), consistent with results observed in the *in vitro* studies with cell lines (Fig. 4). Interestingly, olaparib alone led to an induction of AKT phosphorylation *in vivo* (Fig. 6F), an observation consistent with an increased FDG uptake in olaparib-treated tumors (Supplementary Fig. S3) as opposed to NVP-BKM120 or the combination, both of which strongly reduced FDG uptake (Fig. 2; Supplementary Figs. S2 and S3).

To examine if there was a pharmacokinetic interaction between NVP-BKM120 and olaparib, we examined NVP-BKM120 levels in animals treated with NVP-BKM120 at 30 mg/kg/d and the combination of NVP-BKM120 and olaparib (30 mg/kg/d and 50 mg/kg/d, respectively). For these studies, tissue extracts were processed for mass spectrometry 3 hours after the last dose (Figs. 6G, Supplementary Fig. S5). We found that although NVP-BKM120 levels in tumor tissues were variable, they were consistently in the micromolar range and were not affected by concurrent administration of olaparib.

The mouse model used here for *BRCA1*-related breast cancer MMTV-Cre*Brca1*$^{f/f}$*Trp53*$^{+/-}$ results in the residual expression of a hypomorphic BRCA1 protein, and we did find residual Rad51 recruitment to repair foci (Fig. 5C). This residual homologous recombination activity may also explain the incomplete responses of the BRCA1-exon 11–deleted–expressing mammary tumors to olaparib monotherapy (Fig. 6C).

To test the applicability of our results to human *BRCA1*-related breast cancer, we treated xenograft tumors established from patients with *BRCA1*-related breast cancer (Fig. 6H and I). The first patient-derived tumor (Fig. 6H) was derived from a patient with an N-terminal germline mutation in *BRCA1* (185 del AG). At the time of tissue acquisition, this tumor had developed resistance to standard chemotherapy as well as olaparib, which had been administered in the context of a clinical trial. Growth of this tumor was modestly attenuated by either NVP-BKM120 or olaparib alone in HsdCpb:NMRI-Foxn1nu (nude) mice. However, the combination induced stability over a period of 8 weeks (Fig. 6H), confirming the *in vivo* synergy that we observed in our genetically engineered mouse model of *BRCA1*-related breast cancer. The second human tumor (Fig. 6I) was derived from a patient with a C-terminal *BRCA1* germline mutation (2080 del A). The patient who donated this tumor specimen had not yet been treated, and the tumor showed exquisite sensitivity to the PARP inhibitor, NVP-BKM120, and the combination of both drugs. These human *ex vivo* data confirm the sensitivity of *BRCA1*-related breast cancer to NVP-BKM120, olaparib, and their combination, and, taken together, justify the exploration of this combination in an early-phase clinical trial.

Resistance to Treatments that Include PI3K Inhibitors Occurs at the "Pushing Margin" and Is Associated with ERK Phosphorylation

Eventually, even in tumors that received dual treatments, resistance was observed and at that point, tumors regrew rapidly (Fig. 6A–D). To determine the nature of resistance to the NVP-BKM120 and olaparib combination, we examined pretreatment biopsies, on-treatment biopsies at the time of response on day 10, and posttreatment tissue at the time of progression (Fig. 7A). Target inhibition, that is, suppression of AKT phosphorylation, was maintained even in resistant tumors (Fig. 7A, panel 1), suggesting that resistance to NVP-BKM120 is not due to PI3K pathway activation but to relief of feedback inhibition of alternative pathways, including MAPK activation as suggested earlier (31). The "pushing margin," that is, a highly proliferative rim of tumor cells that rarely infiltrate the surrounding tissue, is a hallmark of *BRCA1*-related tumors (38), yet its biologic basis is not understood. Interestingly, we found an increase in the number of cells with high phospho-ERK levels especially at the "pushing margin" of the tumor, paralleled by an increase in proliferating, that is, Ki67-positive cells (Fig. 7A and B, Supplementary Fig. S6). This phenomenon, the concentration of phosphorylated ERK (p-ERK)–positive cells at the "pushing margin," was seen in tumors before treatment (Fig. 4B, Fig. 7A), at the time of progression on NVP-BKM120 alone (Fig. 4B), or at the time of progression on the combination of the PARP inhibitor with NVP-BKM120, whereas in responding tumors (day 10 biopsy), p-ERK–positive cells were conspicuously absent (Fig. 7A). As expected with PI3K inhibition and consistent with the p-ERK status of tumor cells, we found that tumors initially showed a stark decrease in proliferative activity (Ki67, Fig. 7A

Published OnlineFirst August 22, 2012; DOI:10.1158/2159-8290.CD-11-0336

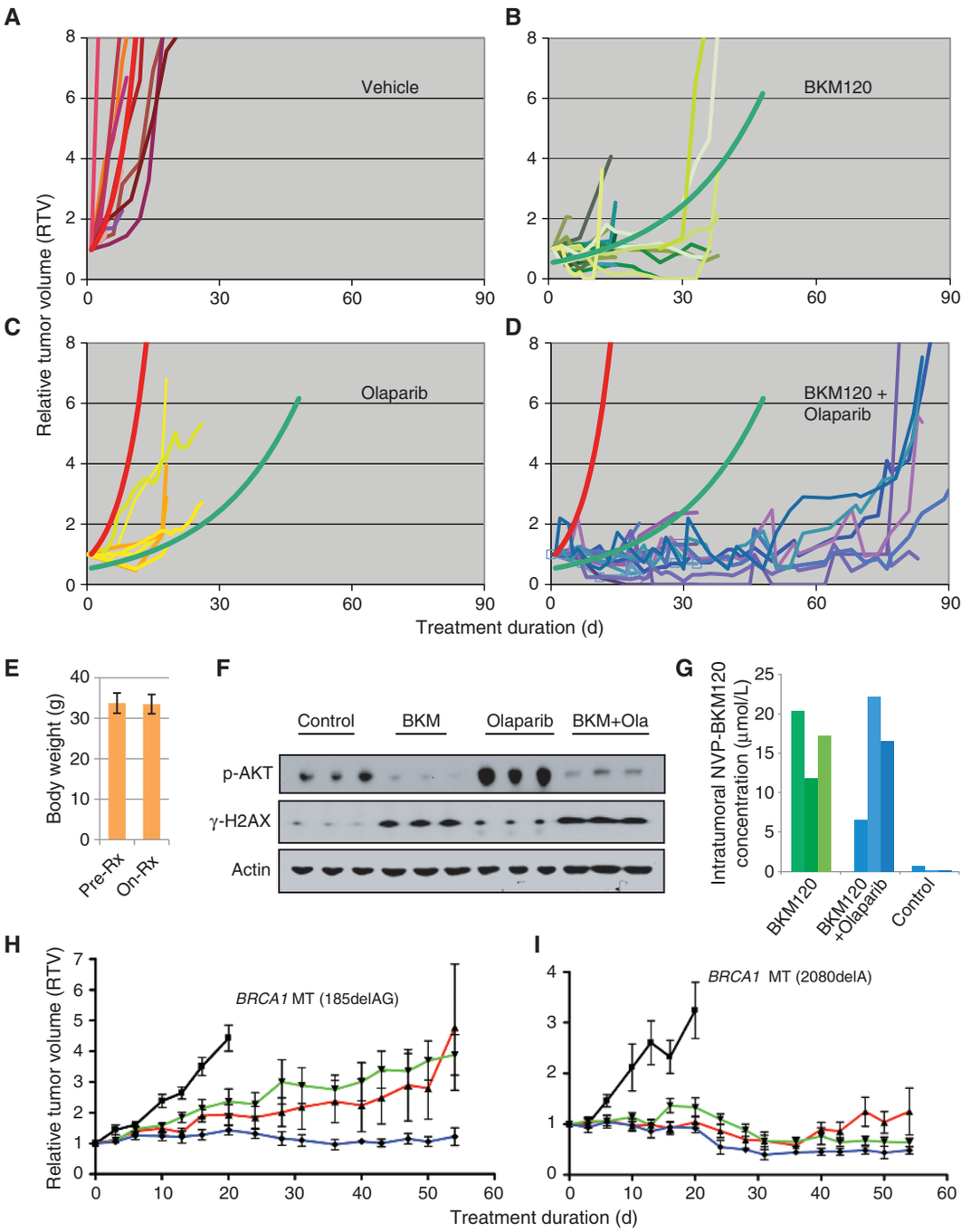

Figure 6. Antitumor efficacy of PI3K inhibitor NVP-BKM120 alone and in combination with olaparib. **A–D,** tumor-bearing MMTV-Cre*Brca1*$^{f/f}$*Trp53*$^{+/-}$ were treated with either vehicle control (**A**), NVP-BKM120 [**B,** 50 mg/kg/d ($n = 11$) or 30 mg/kg/d ($n = 10$)], olaparib [**C,** 50 mg/kg/d ($n = 8$)] or the combination of NVP-BKM120 and olaparib [**D,** NVP-BKM 50 mg/kg/d + olaparib 50 mg/kg/d ($n = 8$) or NVP-BKM 30 mg/kg/d + olaparib 50 mg/kg/d ($n = 7$)], and tumor volumes were measured every 2 to 3 days using calipers. Trend lines for vehicle control (red curve) and NVP-BKM120 treatments (green curve) were calculated using all data points to determine best fit. The functions of the best-fit curves were used to determine tumor-doubling times for all 3 treatment modalities and controls. **E,** stable body mass with PI3K inhibitor and PARP inhibitor treatments. Mice were weighed before and after treatments. **F** and **G,** target inhibition and pharmacokinetics *in vivo*. Tumor tissues harvested from animals treated with NVP-BKM120 (30 mg/kg/d) alone or in combination with olaparib (50 mg/kg/d) as indicated were harvested 3 hours after the last treatment and subjected to immunoblotting with antibodies against actin, p-AKT, and γ-H2AX (**F**) or lysed and subjected to mass spectrometry (**G**). For standards used, see Methods and Supplementary Fig. S5. **H** and **I**, responses of human *BRCA1*-related breast cancers implanted as xenotransplants into nude mice to NVP-BKM120, olaparib, or their combination. Breast cancer tissues from 2 patients, one with a 185delAG germline mutation (**H**) and the other one with a 2080delA germline mutation (**I**) were propagated as subcutaneous implants in nude mice. Tumors were allowed to grow to a size of 5 mm when mice were randomized to treatments with either vehicle control (black), NVP-BKM120 (red), olaparib (green), or their combination [blue ($n = 6$ for each cohort, same dosing as in F)]. Tumor assessment with electronic calipers was done as described in Methods.

Published OnlineFirst August 22, 2012; DOI:10.1158/2159-8290.CD-11-0336

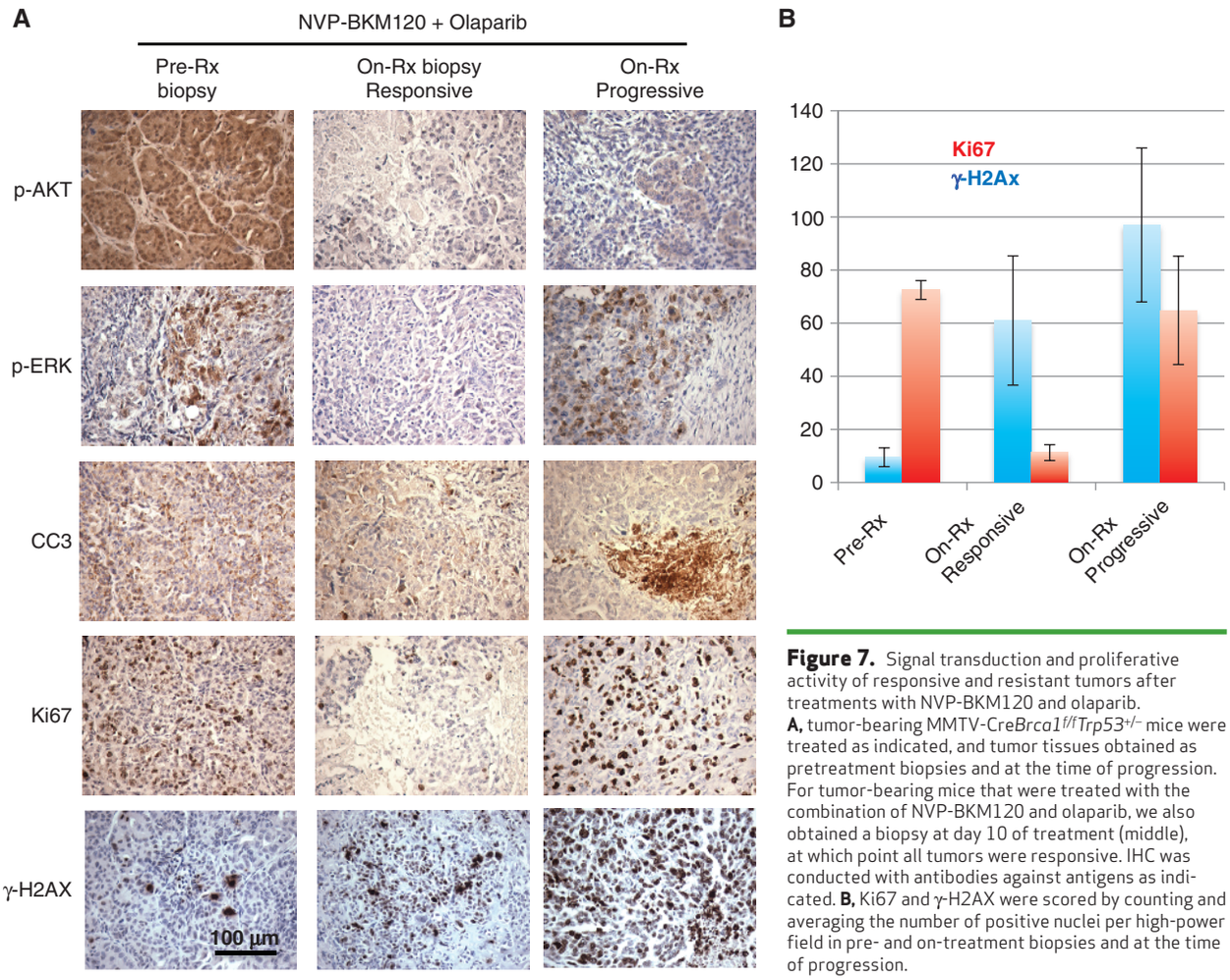

Figure 7. Signal transduction and proliferative activity of responsive and resistant tumors after treatments with NVP-BKM120 and olaparib. **A,** tumor-bearing MMTV-Cre*Brca1*$^{f/f}$*Trp53*$^{+/-}$ mice were treated as indicated, and tumor tissues obtained as pretreatment biopsies and at the time of progression. For tumor-bearing mice that were treated with the combination of NVP-BKM120 and olaparib, we also obtained a biopsy at day 10 of treatment (middle), at which point all tumors were responsive. IHC was conducted with antibodies against antigens as indicated. **B,** Ki67 and γ-H2AX were scored by counting and averaging the number of positive nuclei per high-power field in pre- and on-treatment biopsies and at the time of progression.

and B), and that resistant tumors were characterized by high mitotic activity (Figs. 4B, 7A and B). Thus, the activation of proproliferative MAPK signaling may be a major driver for the resistance of tumors treated with PI3K inhibitors.

DISCUSSION

We report here on a surprising *in vivo* synergy of NVP-BKM120 in combination with olaparib for the treatment of *BRCA1*-mutant breast tumors, which suggests an important role of PI3Kα in the DNA damage response. Kumar and colleagues (39) showed that PI3K β is required for the recruitment of NBS1 to DNA DSBs and for the assembly of repair foci in response to ionizing radiation. It was shown previously that loss of PTEN, frequently seen in TNBC, leads not only to activation of the PI3K pathway, but also to an accumulation of DNA DSBs (40). In addition, NVP-BKM120 enhances production of PAR and phosphorylation of H2AX, suggesting increased DNA damage when the PI3K pathway is inhibited in the context of a *BRCA1* mutation. *In vivo* H2AX phosphorylation in tumors increased when mice were treated with the combination of NVP-BKM120 and olaparib during the period of response (day 10), and was highest at the time of treatment failure (Fig. 7), suggestive of a progressive accumulation of unrepaired DNA DSBs, which would contribute to the reliance on PARP activity for DNA damage repair and would explain the sensitivity to combined PARP and PI3K inhibtion.

Of particular interest was our observation that, despite the increase in phosphorylation of H2AX in response to NVP-BKM120, both NVP-BKM120 and depletion of PI3Kα greatly reduced Rad51 incorporation into foci in cells treated with radiation. These results suggest that class IA PI3K catalytic activity is required for recruitment of Rad51 into sites of DNA damage and raise the possibility that the increase in DNA-PK phosphorylation is a feedback response to this failure to form proper DNA damage repair complexes. *BRCA1* is known to play a role in recruitment of Rad51 to sites of DNA damage (41), and thus it is possible that in *BRCA1*-defective cells, a PI3K-dependent pathway becomes more critical for this recruitment. Clearly, additional studies will be needed to understand the interactions between PI3K, Rad51, and DNA-PK in DNA repair processes.

Regulated PARP activity allows for DNA damage repair required for the maintenance of genomic stability. However, massive PARP activation leads to the depletion of its substrate NAD^+ and consecutively depletion of ATP in an effort to replenish NAD^+, resulting in energy loss and eventually cell death. Activation of PI3Kα leads to increased energy

Published OnlineFirst August 22, 2012; DOI:10.1158/2159-8290.CD-11-0336

production via glycolysis. Glycolysis and PAR both consume NAD^+, and may compete for NAD^+ available in the cytosol. Such metabolic competition makes sense for decisions on the fate of cells: if energy supply and glycolysis are high, the amount of NAD^+ diverted into PAR is limited, and cell death as a consequence of massive PARP activation is avoided. Conversely, if glucose supply and glycolytic activity are low, NAD^+ is consumed by PARP, and the ensuing massive PAR may lead to cell death (42). PARP inhibition spares NAD^+, which becomes available for glycoloysis and can protect cells from death, such as myocardial or central nervous system ischemia (43, 44), sepsis (45), or pancreatic islet cell damage (46). Consistent with this model, we saw *in vivo* enhancement of glucose uptake (Supplementary Fig. S3) and phosphorylation of AKT in response to PARP inhibition, which was reversed by addition of the PI3K inhibitor (Fig. 6E). Thus, a possible explanation for the *in vivo* synergy of PI3K and PARP inhibitors is that PI3K inhibition reverses the prosurvival effect of PARP inhibition and thereby makes these drugs more effective, a combination that one would predict to be particularly effective in cancers with defects in homologous recombination, such as *BRCA1/2*-related breast and ovarian cancers.

Finally, it is noteworthy that the *in vivo* approach allowed us to make several observations that could not be made *in vitro*: much greater efficacy of the NVP-BKM120/olaparib combination was observed *in vivo* than *in vitro*, suggesting that tumor microenvironment and metabolism may be important. Sequential tumor biopsies allowed us to monitor target inhibition in combination with tumormetrics, which allowed us to discover a potent synergy of the PI3K inhibitor NVP-BKM120 with the PARP inhibitor olaparib to treat *BRCA1*-related breast cancer that may warrant exploration in an early-phase clinical trial.

METHODS

Materials

The PI3K inhibitor NVP-BKM120 was obtained through a Material Transfer Agreement with Novartis Pharmaceuticals. Olaparib was purchased from LC Laboratories and KU-55933 was purchased from Selleck. *BRCA1*-mutant human breast cancer cell line HCC1937 was from American Type Culture Collection, CRL-2336, and maintained in Dulbecco's Modified Eagle's Medium (DMEM)/10% FBS, and SUM149 was a gift from Dr. Christina Gewinner, Division of Signal Transduction, Beth Israel Deaconess Medical Center (Boston, MA), maintained in Ham's F-12 with 5% FBS, 5 μg/mL insulin, 2 μg/mL hydrocortisone, 5 μg/mL gentamicin, and 2.5 μg/mL fungizone. Cell lines were authenticated by immunoblotting for BRCA1 and PTEN and tested for the absence of mycoplasma.

Animal Experimentation

Animal experiments were conducted in accordance with Institutional Animal Care and Use Committee (IACUC)–approved protocols at Beth Israel Deaconess Medical Center, and at the University of Vall d'Hebron (Barcelona, Spain). Female MMTV-Cre*Brca1*$^{f/f}$*Trp53*$^{+/-}$ mice were obtained by breeding *Brca1* conditional knockout mice (01XC8, strain C57BL/6), originally generated by Drs. Xiaoling Xu and Chu-Xia Deng (12), who made these mice available to us via the National Cancer Institute (NCI) repository with MMTV-Cre [Jackson Laboratory B6129-TgN (MMTV-Cre) 4Mam; ref. 47)] and *Trp53* knockout (Taconic Farms, P53N12-M, C57BL/6; ref. 48). At the time of the study, mice had been inbred for 4 years (>7 generations). The floxed or wild-type status of *Brca1*, the presence of the MMTV-Cre transgene, and the *Trp53* heterozygosity were determined by PCR as previously described (12). Mice were examined for the occurrence of tumors twice weekly. When tumormetrics were conducted, the length and width of the tumor was determined using calipers, and the tumor volume was determined (width^2 × length/2). Tumor volume was used as a measure of growth and was recorded as ratio to tumor volume at diagnosis. Tumor doubling times were calculated using the functions of the best-fit curves for all data points in each treatment modality. NVP-BKM120 was resuspended in 5% methylcellulose solution (Fluka) and administered via oral gavage at 50 mg/kg/d or 30 mg/kg/d. Olaparib was resuspended for intraperitoneal administration as described (15) and dosed at 50 mg/kg/d. For patient-derived tumor grafts, consent for tumor use was obtained from patients under a protocol approved by the Vall d'Hebron Hospital Clinical Investigation Ethical Committee. Tumors were subcutaneously implanted in 6-week-old female HsdCpb:NMRI-Foxn1nu mice (Harlan Laboratories, Italy). Animals were supplemented with 1 μmol/L estradiol (Sigma) in the drinking water. After tumor graft growth, tumor tissue was reimplanted into recipient mice, which were randomized upon implant growth.

FDG-PET Scanning

A total of 0.3 to 0.4 mCi of FDG was injected intravenously through the retro-orbital vein of the anesthetized mouse. After a "washout" period of 1 hour, the mouse was imaged on a NanoPET/CT (Bioscan/Mediso) scanner. The NanoPET/CT is a high-resolution small-animal multimodality scanner consisting of 12 lutetium yttrium oxyorthosilicate (LYSO) detector blocks. The blocks comprise a total of 39,780 crystals each with a dimension of 1.2 mm × 1.2 mm × 13 mm^3.

Images were acquired in 3 dimensions. The mice remained supine and maintained their position throughout the procedure. First, a computed tomography (CT) scan was conducted, and second, a whole-body FDG-PET scan was acquired covering the same area as the CT scan. Counts per minute (cpm) were obtained, converted to mCi, and values were normalized for region of interest volume and injected dose. To correct for metabolic variability between exams and to determine tumor-specific uptake changes, FDG-uptake rates were corrected for cardiac FDG uptake (μCi/μCi injected/voxels^{tumor})/(μCi/μCi injected/voxels^{heart}). For studies involving repeat scanning, the change in tumor-specific FDG uptake was determined in percentage [1 − (FDG-uptake^{post}/FDG-uptake^{pre}) ×100]. Animals were housed in the Longwood Small Animal Imaging Facility between scans.

Immunohistochemistry

For immunohistochemistry (IHC), we used anti-CC3 (9661S, Cell Signalling, Rabbit polyclonal Asp175) and anti-Ki67 (9106-S; Thermo Scientific, Rabbit monoclonal SP6). All other antibodies used are described in Immunoblotting. All IHCs were done as described previously (11), including antigen retrieval with a citrate-buffer.

Immunoblotting

Cells were treated with mock, NVP-BKM120, olaparib, KU-55933, or the combination and lysed in cell lysis buffer (9803, Cell Signaling) per the manufacturer's instructions. Immunoblots were conducted using the Nupage System (Invitrogen). A total of 20 μg of protein was loaded, except for PAR, phospho-ATM, and phospho-DNA-PK/PRKDC Western blot analysis, where 40 μg were loaded. Tumor tissue lysates were prepared similarly with the exception of tissue homogenization by using an electric homogenizer for 30 milliseconds after addition of the lysis buffer. Primary antibodies used for Western blot analysis were total AKT (9272), CC3 (9661), total ERK (4695), phosphorylated AKT Ser473 (4058), phosphorylated ERK Thr202/Tyr204

Published OnlineFirst August 22, 2012; DOI:10.1158/2159-8290.CD-11-0336

(9106), phosphorylated histone H2AX Ser139 (2577), and PTEN (9559) from Cell Signaling. Phospho-ATM Ser1981 (2152-1) and phospho-DNA-PK/PRKDC Ser2056 (3892-1) were obtained from Epitomics; CD31 (ab28364), actin (ab6276), and INPP4B (ab81269) from Abcam; pADPr (sc56198) from Santacruz Biotechnology; and Ki67 (RM-9106) was purchased from Thermo Scientific. Rad51 antibody was a gift from Dr. Ralph Scully.

Immunofluorescence

Cells were plated on coverslips in 6-well plates and incubated overnight at 37°C with 5% CO_2 before drug treatment. Cells were exposed to NVP-BKM-120 for 24 hours followed by irradiation (10 Gy). Cells were fixed with 3% paraformaldehyde and 2% sucrose diluted in PBS 6 hours postirradiation and subsequently permeabilized with 0.5% TritonX-100 buffer (20 mmol/L HEPES pH 7.4, 50 mmol/L NaCl, 3 mmol/L MgCl, and 300 mmol/L sucrose) for 3 minutes on ice. Cells were incubated with a primary rabbit antihuman Rad-51 antiserum at 1:500 dilution in hybridization buffer (5% goat serum, 0.5% NaN_3, 1 × PBS) for 30 minutes at 37°C. Secondary antibody used was a donkey antirabbit Alexafluor 488 conjugate (Invitrogen) at a concentration of 1:50. Images were acquired using a Zeiss 710 NLO laser scanning confocal microscope.

siRNA Transfections

The siRNAs were obtained from Dharmacon. SUM149 cells were transfected with either 10 or 30 nmol/L pool of 4 siRNA sequences targeting PIK3CA (catalog number L-003018-00-0005) or PIK3CB (catalog number L-003019-00-0005) siRNA using HiPerFect Transfection Reagent (QIAGEN) according to the manufacturer's protocol. Control cells were treated with HiPerFect alone. Cells were grown and harvested 48 hours after the transfection using cell lysis buffer (9803, Cell Signaling) per the manufacturer's instructions and analyzed by immunoblotting.

Cell Viability Assay

For cell viability assays, breast cancer cells were seeded at a density of 250 cells per well in 96-well plates in the absence or presence of drugs, and cell viability was determined using the CellTiter-Glo Luminescent Cell Viability Assay (Promega) according to the manufacturer's instructions, using a Wallac 3 plate reader.

Sequencing

Genomic DNA was isolated and PCR amplification conducted for regions in the murine *Pik3ca* gene that are homologous to the regions frequently mutated in human breast cancer, that is, E542K and E545K in the helical domain and H1047R in the kinase domain. Primers used were for exon 9: forward CGCATACCTGCATCTGTTCTA; reverse AAATGATGTGTGTGCTGGGT, exon 20: forward AGCAGCTCACTGACCAGATGT; reverse ACTCACTGCCATGCAGTGGA. PCR products were subjected to direct sequencing at Genewiz.

Data Analysis

Determination of the Chalkley score was done as described (29, 49). Briefly, the 3 most vascular areas (hot spots) with the highest number of microvessel profiles in each tumor were photographed under an Olympus light microscope at × 200; a digital mask representing the Chalkley grid area, 0.196 mm^2, was used to count the CD31-positive spots in a blind fashion and the mean value of the 3 grid counts was obtained. A 2-sided *t* test was used to determine significance.

Targeted Mass Spectrometry (LC/MS-MS) for BKM120 Pharmacokinetics Study

Metabolites from 100 mg of mouse tumor samples were extracted using 80% methanol according to Yuan and colleagues (50), and 10 μL were injected and analyzed using a 5500 QTRAP hybrid triple quadrupole mass spectrometer (AB/SCIEX) coupled to a Prominence UFLC HPLC system (Shimadzu) via selected reaction monitoring for the Q1/Q3 transition of 410.8/367.0 for NVP-BKM120. ESI voltage was +4,900 V in positive ion mode using a dwell time of 4 milliseconds and collision energy of 45. Approximately 15 data points were obtained for NVP-BKM120 per liquid chromatography/tandem mass spectrometry (LC/MS-MS) experiment. Samples were delivered to the MS via hydrophilic interaction chromatography (HILIC) using a 4.6 mm i.d. × 10 cm Amide Xbridge column (Waters) at 350 μL/min. Gradients were run starting from 85% buffer B (HPLC grade acetonitrile) to 42% B from 0 to 5 minutes; 42% B to 0% B from 5 to 16 minutes; 0% B was held from 16 to 24 minutes; 0% B to 85% B from 24 to 25 minutes; and 85% B was held for 7 minutes to reequilibrate the column. NVP-BKM120 eluted at approximately 3.50 minutes. Buffer A was composed of 20 mmol/L ammonium hydroxide/20 mmol/L ammonium acetate (pH 9.0) in 95:5 water:acetonitrile. Peak areas from the total ion current for the NVP-BKM120 metabolite selected reaction monitoring transition was integrated using MultiQuant v2.0 software (AB/SCIEX). For the concentration curve data, NVP-BKM120 was prepared at concentrations of 1 nmol/L, 10 nmol/L, 100 nmol/L, 500 nmol/L, 1 μmol/L, and 10 μmol/L in 40% methanol. Five microliters of each sample were injected using the parameters described earlier.

Disclosure of Potential Conflicts of Interest

L.C. Cantley and J. Baselga have consulted for Novartis Pharmaceuticals, which is developing NVP-BKM120 for cancer treatment, and both authors are consultant/advisory board members of Novartis. J. Baselga has consulted for AstraZeneca, which is developing olaparib for cancer treatment. J. Balmañà is a consultant/advisory board member of Clovis. No potential conflicts of interest were disclosed by the other authors.

The Editors-in-Chief of *Cancer Discovery* are the authors of this article. In keeping with the AACR's Editorial Policy, the paper was peer reviewed and a member of the AACR's Publications Committee rendered the decision concerning acceptability.

Authors' Contributions

Conception and design: A. Juvekar, R. Scully, L.C. Cantley, G.M. Wulf

Development of methodology: A. Juvekar, L.N. Burga, H. Hu, Y.H. Ibrahim, A. Papa, G.M. Wulf

Acquisition of data (provided animals, acquired and managed patients, provided facilities, etc.): A. Juvekar, L.N. Burga, E.P. Lunsford, Y.H. Ibrahim, J. Balmañà, A. Rajendran, K. Spencer, C.A. Lyssiotis, C. Nardella, J. Baselga, J.M. Asara, G.M. Wulf

Analysis and interpretation of data (e.g., statistical analysis, biostatistics, computational analysis): A. Juvekar, L.N. Burga, H. Hu, E.P. Lunsford, Y.H. Ibrahim, P.P. Pandolfi, J. Baselga, R. Scully, J.M. Asara, L.C. Cantley, G.M. Wulf

Writing, review, and/or revision of the manuscript: A. Juvekar, L.N. Burga, E.P. Lunsford, C.A. Lyssiotis, C. Nardella, P.P. Pandolfi, J.M. Asara, L.C. Cantley, G.M. Wulf

Administrative, technical, or material support (i.e., reporting or organizing data, constructing databases): E.P. Lunsford, A. Rajendran, A. Papa, G.M. Wulf

Study supervision: A. Papa, L.C. Cantley, G.M. Wulf

Acknowledgments

The authors thank the women who allowed us to study their tumor tissues. We are grateful to Min Yuan for help with mass spectrometry experiments. The authors also thank Novartis Pharmaceuticals for providing NVP-BKM120, Dr. Celina Garcia-Garcia, University Hospital Vall d'Hebron, for her work in the tissue collection study, and

Published OnlineFirst August 22, 2012; DOI:10.1158/2159-8290.CD-11-0336

Drs. Ursula Matulonis and Eric Winer, Dana-Farber Cancer Institute, for their support and discussion of the data.

Grant Support

L.C. Cantley and G.M. Wulf are supported by a Stand Up To Cancer Dream Team Translational Research Grant, a Program of the Entertainment Industry Foundation (SU2C-AACR-DT0209), and by the Breast Cancer Research Foundation (BCRF). G.M. Wulf was supported by a Susan G. Komen for the Cure grant BCTR0601030. J.M. Asara is supported by NIH NCI grants 5P01CA120964-05 and 5P30CA006516-46. L.C. Cantley is supported by NIH grant GM41890 and NCI grant P01CA089021.

Received December 21, 2011; revised July 1, 2012; accepted August 8, 2012; published OnlineFirst August 22, 2012.

REFERENCES

1. Gayther SA, Warren W, Mazoyer S, Russell PA, Harrington PA, Chiano M, et al. Germline mutations of the BRCA1 gene in breast and ovarian cancer families provide evidence for a genotype–phenotype correlation. Nat Genet 1995;11:428–33.
2. Tutt A, Robson M, Garber JE, Domchek SM, Audeh MW, Weitzel JN, et al. Oral poly(ADP-ribose) polymerase inhibitor olaparib in patients with BRCA1 or BRCA2 mutations and advanced breast cancer: a proof-of-concept trial. Lancet 2010;376:235–44.
3. Fong PC, Boss DS, Yap TA, Tutt A, Wu P, Mergui-Roelvink M, et al. Inhibition of poly(ADP-ribose) polymerase in tumors from BRCA mutation carriers. N Engl J Med 2009;361:123–34.
4. Audeh MW, Carmichael J, Penson RT, Friedlander M, Powell B, Bell-McGuinn KM, et al. Oral poly(ADP-ribose) polymerase inhibitor olaparib in patients with BRCA1 or BRCA2 mutations and recurrent ovarian cancer: a proof-of-concept trial. Lancet 2010;376:245–51.
5. Fong PC, Yap TA, Boss DS, Carden CP, Mergui-Roelvink M, Gourley C, et al. Poly(ADP)-ribose polymerase inhibition: frequent durable responses in BRCA carrier ovarian cancer correlating with platinum-free interval. J Clin Oncol 2010;28:2512–9.
6. Collins LC, Martyniak A, Kandel MJ, Stadler ZK, Masciari S, Miron A, et al. Basal cytokeratin and epidermal growth factor receptor expression are not predictive of BRCA1 mutation status in women with triple-negative breast cancers. Am J Surg Pathol 2009;33:1093–7.
7. van der Groep P, Bouter A, van der Zanden R, Siccama I, Menko FH, Gille JJ, et al. Distinction between hereditary and sporadic breast cancer on the basis of clinicopathological data. J Clin Pathol 2006;59:611–7.
8. Maor S, Yosepovich A, Papa MZ, Yarden RI, Mayer D, Friedman E, et al. Elevated insulin-like growth factor-I receptor (IGF-IR) levels in primary breast tumors associated with BRCA1 mutations. Cancer Lett 2007;257:236–43.
9. Neuhausen SL, Brummel S, Ding YC, Steele L, Nathanson KL, Domchek S, et al. Genetic variation in IGF2 and HTRA1 and breast cancer risk among BRCA1 and BRCA2 carriers. Cancer Epidemiol Biomarkers Prev 2011;20:1690–702.
10. Neuhausen SL, Brummel S, Ding YC, Singer CF, Pfeiler G, Lynch HT, et al. Genetic variation in insulin-like growth factor signaling genes and breast cancer risk among BRCA1 and BRCA2 carriers. Breast Cancer Res 2009;11:R76.
11. Burga LN, Hu H, Juvekar A, Tung NM, Troyan SL, Hofstatter EW, et al. Loss of BRCA1 leads to an increase in epidermal growth factor receptor expression in mammary epithelial cells, and epidermal growth factor receptor inhibition prevents estrogen receptor-negative cancers in BRCA1-mutant mice. Breast Cancer Res 2011;13:R30.
12. Xu X, Wagner KU, Larson D, Weaver Z, Li C, Ried T, et al. Conditional mutation of Brca1 in mammary epithelial cells results in blunted ductal morphogenesis and tumour formation. Nat Genet 1999;22:37–43.
13. Brodie SG, Xu X, Qiao W, Li WM, Cao L, Deng CX. Multiple genetic changes are associated with mammary tumorigenesis in Brca1 conditional knockout mice. Oncogene 2001;20:7514–23.
14. Shukla V, Coumoul X, Cao L, Wang RH, Xiao C, Xu X, et al. Absence of the full-length breast cancer-associated gene-1 leads to increased expression of insulin-like growth factor signaling axis members. Cancer Res 2006;66:7151–7.
15. Rottenberg S, Jaspers JE, Kersbergen A, van der Burg E, Nygren AO, Zander SA, et al. High sensitivity of BRCA1-deficient mammary tumors to the PARP inhibitor AZD2281 alone and in combination with platinum drugs. Proc Natl Acad Sci U S A 2008;105:17079–84.
16. Xiang T, Ohashi A, Huang Y, Pandita TK, Ludwig T, Powell SN, et al. Negative regulation of AKT activation by BRCA1. Cancer Res 2008;68:10040–4.
17. Razandi M, Pedram A, Rosen EM, Levin ER. BRCA1 inhibits membrane estrogen and growth factor receptor signaling to cell proliferation in breast cancer. Mol Cell Biol 2004;24:5900–13.
18. Yan Y, Haas JP, Kim M, Sgagias MK, Cowan KH. BRCA1-induced apoptosis involves inactivation of ERK1/2 activities. J Biol Chem 2002;277:33422–30.
19. Saal LH, Gruvberger-Saal SK, Persson C, Lovgren K, Jumppanen M, Staaf J, et al. Recurrent gross mutations of the PTEN tumor suppressor gene in breast cancers with deficient DSB repair. Nat Genet 2008;40:102–7.
20. Gewinner C, Wang ZC, Richardson A, Teruya-Feldstein J, Etemadmoghadam D, Bowtell D, et al. Evidence that inositol polyphosphate 4-phosphatase type II is a tumor suppressor that inhibits PI3K signaling. Cancer Cell 2009;16:115–25.
21. Fedele CG, Ooms LM, Ho M, Vieusseux J, O'Toole SA, Millar EK, et al. Inositol polyphosphate 4-phosphatase II regulates PI3K/Akt signaling and is lost in human basal-like breast cancers. Proc Natl Acad Sci U S A 2010;107:22231–6.
22. Specht JM, Kurland BF, Montgomery SK, Dunnwald LK, Doot RK, Gralow JR, et al. Tumor metabolism and blood flow as assessed by positron emission tomography varies by tumor subtype in locally advanced breast cancer. Clin Cancer Res 2010;16:2803–10.
23. Tafreshi NK, Kumar V, Morse DL, Gatenby RA. Molecular and functional imaging of breast cancer. Cancer Control 2010;17:143–55.
24. Engelman JA, Chen L, Tan X, Crosby K, Guimaraes AR, Upadhyay R, et al. Effective use of PI3K and MEK inhibitors to treat mutant Kras G12D and PIK3CA H1047R murine lung cancers. Nat Med 2008;14:1351–6.
25. Engelman JA, Luo J, Cantley LC. The evolution of phosphatidylinositol 3-kinases as regulators of growth and metabolism. Nat Rev Genet 2006;7:606–19.
26. Vander Heiden MG. Targeting cell metabolism in cancer patients. Sci Transl Med 2010;2:31ed1.
27. Schnell CR, Stauffer F, Allegrini PR, O'Reilly T, McSheehy PM, Dartois C, et al. Effects of the dual phosphatidylinositol 3-kinase/mammalian target of rapamycin inhibitor NVP-BEZ235 on the tumor vasculature: implications for clinical imaging. Cancer Res 2008;68:6598–607.
28. Yuan TL, Choi HS, Matsui A, Benes C, Lifshits E, Luo J, et al. Class 1A PI3K regulates vessel integrity during development and tumorigenesis. Proc Natl Acad Sci U S A 2008;105:9739–44.
29. Fox SB, Leek RD, Weekes MP, Whitehouse RM, Gatter KC, Harris AL. Quantitation and prognostic value of breast cancer angiogenesis: comparison of microvessel density, Chalkley count, and computer image analysis. J Pathol 1995;177:275–83.
30. Maira SM, Pecchi S, Huang A, Burger M, Knapp M, Sterker D, et al. Identification and characterization of NVP-BKM120, an orally available pan-class I PI3-kinase inhibitor. Mol Cancer Ther 2012;11:317–28.
31. Chandarlapaty S, Sawai A, Scaltriti M, Rodrik-Outmezguine V, Grbovic-Huezo O, Serra V, et al. AKT inhibition relieves feedback suppression of receptor tyrosine kinase expression and activity. Cancer Cell 2011;19:58–71.

Published OnlineFirst August 22, 2012; DOI:10.1158/2159-8290.CD-11-0336

32. Tomlinson GE, Chen TT, Stastny VA, Virmani AK, Spillman MA, Tonk V, et al. Characterization of a breast cancer cell line derived from a germ-line BRCA1 mutation carrier. Cancer Res 1998;58:3237–42.
33. Forozan F, Veldman R, Ammerman CA, Parsa NZ, Kallioniemi A, Kallioniemi OP, et al. Molecular cytogenetic analysis of 11 new breast cancer cell lines. Br J Cancer 1999;81:1328–34.
34. Farmer H, McCabe N, Lord CJ, Tutt AN, Johnson DA, Richardson TB, et al. Targeting the DNA repair defect in BRCA mutant cells as a therapeutic strategy. Nature 2005;434:917–21.
35. Hickson I, Zhao Y, Richardson CJ, Green SJ, Martin NM, Orr AI, et al. Identification and characterization of a novel and specific inhibitor of the ataxia-telangiectasia mutated kinase ATM. Cancer Res 2004; 64:9152–9.
36. Drost R, Bouwman P, Rottenberg S, Boon U, Schut E, Klarenbeek S, et al. BRCA1 RING function is essential for tumor suppression but dispensable for therapy resistance. Cancer Cell 2011;20:797–809.
37. Yuan SS, Lee SY, Chen G, Song M, Tomlinson GE, Lee EY. BRCA2 is required for ionizing radiation-induced assembly of Rad51 complex *in vivo*. Cancer Res 1999;59:3547–51.
38. Lakhani SR, Jacquemier J, Sloane JP, Gusterson BA, Anderson TJ, van de Vijver MJ, et al. Multifactorial analysis of differences between sporadic breast cancers and cancers involving BRCA1 and BRCA2 mutations. J Natl Cancer Inst 1998;90:1138–45.
39. Kumar A, Fernandez-Capetillo O, Carrera AC. Nuclear phosphoinositide 3-kinase beta controls double-strand break DNA repair. Proc Natl Acad Sci U S A 2010;107:7491–6.
40. Shen WH, Balajee AS, Wang J, Wu H, Eng C, Pandolfi PP, et al. Essential role for nuclear PTEN in maintaining chromosomal integrity. Cell 2007;128:157–70.
41. Bhattacharyya A, Ear US, Koller BH, Weichselbaum RR, Bishop DK. The breast cancer susceptibility gene BRCA1 is required for subnuclear assembly of Rad51 and survival following treatment with the DNA cross-linking agent cisplatin. J Biol Chem 2000;275:23899–903.
42. Ha HC, Snyder SH. Poly(ADP-ribose) polymerase is a mediator of necrotic cell death by ATP depletion. Proc Natl Acad Sci U S A 1999; 96:13978–82.
43. Zingarelli B, Salzman AL, Szabo C. Genetic disruption of poly (ADP-ribose) synthetase inhibits the expression of P-selectin and intercellular adhesion molecule-1 in myocardial ischemia/reperfusion injury. Circ Res 1998;83:85–94.
44. Eliasson MJ, Sampei K, Mandir AS, Hurn PD, Traystman RJ, Bao J, et al. Poly(ADP-ribose) polymerase gene disruption renders mice resistant to cerebral ischemia. Nat Med 1997;3:1089–95.
45. Soriano FG, Liaudet L, Szabo E, Virag L, Mabley JG, Pacher P, et al. Resistance to acute septic peritonitis in poly(ADP-ribose) polymerase-1-deficient mice. Shock 2002;17:286–92.
46. Masutani M, Suzuki H, Kamada N, Watanabe M, Ueda O, Nozaki T, et al. Poly(ADP-ribose) polymerase gene disruption conferred mice resistant to streptozotocin-induced diabetes. Proc Natl Acad Sci U S A 1999;96:2301–4.
47. Wagner KU, Wall RJ, St-Onge L, Gruss P, Wynshaw-Boris A, Garrett L, et al. Cre-mediated gene deletion in the mammary gland. Nucleic Acids Res 1997;25:4323–30.
48. Donehower LA, Harvey M, Slagle BL, McArthur MJ, Montgomery CA Jr, Butel JS, et al. Mice deficient for p53 are developmentally normal but susceptible to spontaneous tumours. Nature 1992;356:215–21.
49. Fox SB, Turner GD, Leek RD, Whitehouse RM, Gatter KC, Harris AL. The prognostic value of quantitative angiogenesis in breast cancer and role of adhesion molecule expression in tumor endothelium. Breast Cancer Res Treat 1995;36:219–26.
50. Yuan M, Breitkopf SB, Yang X, Asara JM. A positive/negative ion-switching, targeted mass spectrometry-based metabolomics platform for bodily fluids, cells, and fresh and fixed tissue. Nat Protoc 2012;7:872–81.